photonics

MDPI

Communication

Theoretical Study on Dual-Function Optical Phased Array of LiDAR and Optical Wireless Communication Based on Optically Injection-Locked Semiconductor Lasers

Anh-Hang Nguyen, Hyo-Sang Jeong, Hyungsik Shin and Hyuk-Kee Sung *

Department of Electronic and Electrical Engineering, Hongik University, Seoul 04066, Republic of Korea; hannah@mail.hongik.ac.kr (A.-H.N.); hsjeong@mail.hongik.ac.kr (H.-S.J.); hyungsik.shin@hongik.ac.kr (H.S.)
* Correspondence: hksung@hongik.ac.kr

Abstract: Light detection and ranging (LiDAR) and optical wireless communication (OWC) are in high demand and rapidly developing owing to the explosive growth of smart systems that require automotive and mobile devices. Optical phased arrays (OPA) have become a key technology in LiDAR and OWC owing to their nonmechanical beam steering capabilities. However, using separate LiDAR and OWC platforms in one system creates problems, such as spectrum congestion, resource consumption, and high complexity. We propose a dual-function OPA that enables LiDAR and OWC to function on a single platform based on the simultaneous amplitude and phase modulation of optically injection-locked semiconductor lasers. We numerically demonstrated that the primary LiDAR and secondary OWC function simultaneously by independent control of the main and side lobes in the OPA signal. The variation in side lobe levels is controlled at 20 or 25 dB to realize low- and high-level data for OWC function as well as maintaining the main beam LiDAR function. We successfully achieved wide-opening eye patterns of 10 Gbps data transmission of the OWC operation.

Keywords: optical injection locking; optical phased array; LiDAR; optical wireless communication; dual-function

Citation: Nguyen, A.-H.; Jeong, H.-S.; Shin, H.; Sung, H.-K. Theoretical Study on Dual-Function Optical Phased Array of LiDAR and Optical Wireless Communication Based on Optically Injection-Locked Semiconductor Lasers. *Photonics* **2023**, *10*, 498. https://doi.org/10.3390/photonics10050498

Received: 17 March 2023
Revised: 18 April 2023
Accepted: 25 April 2023
Published: 26 April 2023

1. Introduction

Optical phased arrays (OPA) are an emerging technology for generating and steering optical beams by controlling the amplitude and phase of arrayed optical emitters [1]. Specifically, non-mechanical beam steering based on electronic modulation in OPA elements is a remarkable property that significantly reduces the size, weight, and power consumption [2,3]. The use of a high-frequency optical spectrum is another strength of the OPA compared with the RF spectrum owing to its broad bandwidth, free spectrum license, and interference immunity, which overcome the challenges of the RF spectrum limitations caused by the rapid growth of wireless technologies [4]. Furthermore, OPA of shorter wavelengths compared with RF technology enable a small form factor with large-scale element integration to achieve a narrow beamwidth and high output power. These properties are required for high resolution and fidelity in ranging, sensing, and communication applications [5,6]. Consequently, the OPA is a promising technology that has been extensively developed for applications such as light detection and ranging (LiDAR) [7–9], optical wireless communication (OWC) [10], and medical imaging [11].

Among these applications, LiDAR has been widely adopted in various fields, such as civil, military, agriculture, and medicine applications, owing to its abilities of accurate ranging, velocity mapping, object imaging, and sensing [7]. OWC technology is a candidate for overcoming the ever-growing demand and outstripping the supply of RF wireless communication owing to the use of optical signals for data transmission [4]. Furthermore, the growing demand for automotive devices, such as autonomous vehicles, drones, and mobile robots, requires the simultaneous operation of sensing and communication on

a single platform [12,13]. However, the coexistence of the LiDAR and OWC functions on a single platform results in high complexity and resource consumption. Moreover, LiDAR and OWC operations based on OPA technology utilize a main beam, resulting in a significant power loss in the side lobes. The side lobes are inevitably produced by main beam construction. Consequently, the utilization of side lobes and the main beam is a potential solution to overcome the aforementioned issues.

In this study, we propose an approach for the dual-function operations of a LiDAR and an OWC on a single OPA platform based on optically injection-locked (OIL) semiconductor lasers. To enable dual-function operations, the main beam for LiDAR function needs to be encoded as an AMCW (amplitude-modulated continuous wave), while the side lobes should be amplitude-modulated, with high and low levels of OWC transmission. The proposed dual-function OPA system operates based on the simultaneous amplitude (AM) and phase (PM) modulation abilities of OIL lasers. This enables precise control of the far-field beam pattern for independent modulation between the main beam and side lobes [14]. We previously reported that the amplitudes and phases of OIL-based OPA elements can be simultaneously controlled through the direct modulation of SLs [15,16]. Based on this property, we propose that the OIL-based OPA can simultaneously provide main beam steering for the LiDAR function and side lobe beam shaping for the OWC function. Dual-function OPAs have various advantages, such as spectral efficiency, prevention of spectrum congestion, and interference mitigation, and are potential candidates for automotive applications and Internet of Things systems.

First, we introduce the concept of a dual-function OPA based on an OIL semiconductor laser. This dual function is realized by the direct AM/PM of the OIL lasers. Using the AM and PM in each OPA element, we can achieve side lobe-level (SLL) control of the far-field pattern for data transmission (OWC function), while simultaneously controlling the main lobe for ranging and sensing (LiDAR function). Second, we explain the numerical method for the OIL rate equations and demonstrate the simultaneous AM/PM of OIL semiconductor lasers. Third, we present the far-field beam and eye patterns of data transmission.

2. Concept of Dual-Function OPA Based on OIL Semiconductor Lasers

Figure 1 illustrates the dual-function OPA concept of spectrum and platform sharing. The dual functions are primary LiDAR and secondary OWC. The proposed dual-function OPA is developed using an OIL-based OPA system. We previously reported a LiDAR operation with reduced SLL [15] and an OWC operation with improved security performance [16]. As shown in Figure 1, an OIL-based OPA comprises a single ML and an array of SLs that can be directly amplitude- and phase-modulated through optical injection locking. The ML output is at a frequency of f_{ML}, an amplitude of A_{ML}, and a phase of ϕ_{ML}. The free-running SL output (=without ML injection) is at a frequency of $f_{free,SL}$, an amplitude of $A_{free,SL}$, and a phase of $\phi_{free,SL}$. We define the detuning frequency $\left(\Delta f = f_{ML} - f_{free,SL}\right)$ as the frequency difference between ML and SL, and the injection ratio $\left(R = A_{ML}^2 / A_{free,SL}^2\right)$ as the ML and SL squared amplitudes ratio. The detuning frequency and injection ratio are the two injection-locking parameters that determine the locking phenomena. In the injection-locked case, the SL output exhibits phase and frequency synchronization with the ML, hence operating at the ML frequency f_{ML}, and produces a stable locked-amplitude A_n and phase ϕ_n [17]. Therefore, by modulating the two injection-locking parameters in a stable locking regime, we can simultaneously modulate the amplitude A_n and phase ϕ_n of the injection-locked SL output signal. The output of the independently modulated SL array enables shaping and steering of the main and side lobes as desired. Steering of the main beam was achieved based on the phase difference control between the OPA elements. Data transmission in the side lobe magnitude change was achieved based on the amplitude distribution control of the OPA elements. Therefore, the simultaneous AM/PM of OIL lasers is a significant advancement in OIL-based OPA systems that enables the integration

of LiDAR and OWC functions on a single platform, in addition to the high coherence of OIL optical signals for OPA beamforming.

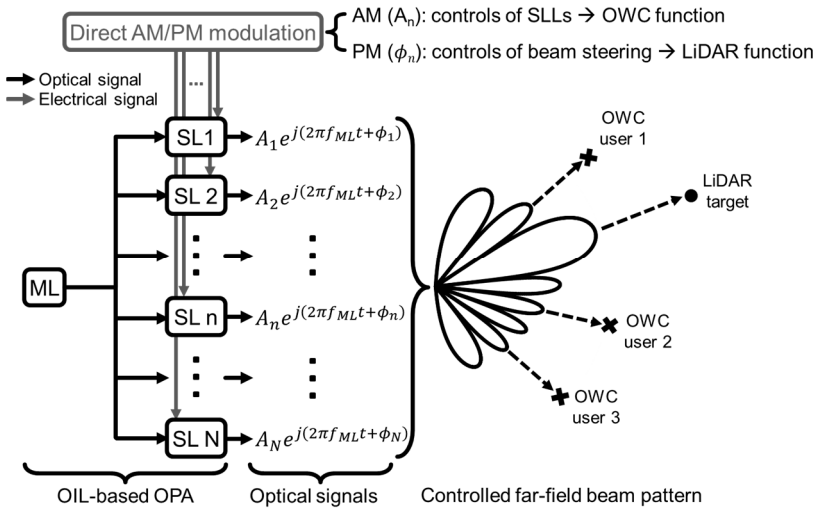

Figure 1. Concept of dual-function optical phased array (OPA) using optically injection-locked (OIL) semiconductor lasers. ML: master laser, SL: slave laser, AM: amplitude modulation, PM: phase modulation, SLL: side lobe level, OWC: optical wireless communication, LiDAR: light detection and ranging.

The OWC function, based on magnitude changes in the side lobes, can be classified into broadcasting and directional communication. In broadcast communication, magnitude changes (e.g., high and low levels) are realized on all side lobes. The data are transmitted simultaneously to multiple OWC receivers located in a spatial area covered by side lobes, as shown in Figure 2a. In directional communication, data are transmitted to OWC receivers located in specific spatial directions, usually for high security demands, as shown in Figure 2b. All side lobes are modulated to identical levels simultaneously in the broadcasting case, whereas only side lobes in specific directions located in the OWC receivers are modulated in the directional OWC case. Because data transmission is based on SLL modulation without affecting the LiDAR operation in the main beam, only the side lobes should be modulated to maintain the main beam power and steering ability, as shown in Figure 2. Because the AM/PM of OIL semiconductor lasers can be achieved through direct current modulation of the SL [15,16], we can achieve SLL modulation for the OWC and power maintenance of the main beam for the LiDAR based on the OIL-based OPA.

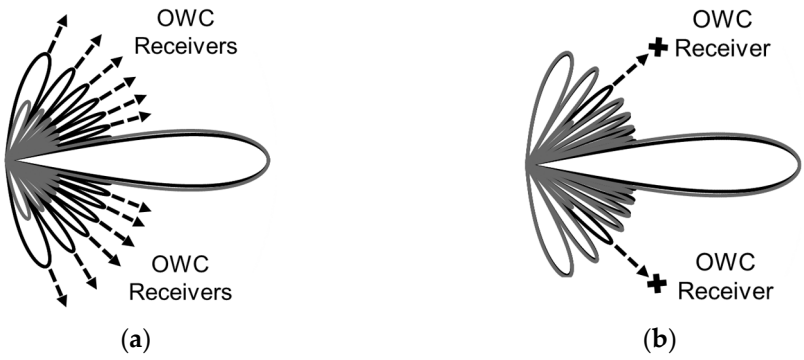

Figure 2. OPA far-field beam patterns showing two scenarios of (**a**) broadcasting and (**b**) directional OWC.

3. Simulation Results

OPA far-field beam patterns are produced by the interference of optical fields with high coherence from the OPA elements. The far-field beam pattern characteristics of the

OIL-based OPA are represented by an array factor (AF), which is derived from the vector addition of the OIL laser outputs and is expressed as in [14,18]:

$$AF(\theta) = \sum_{n=1}^{N} A_n \exp\{j(n-1)(kd\cos\theta + \Delta\phi)\}, \quad (1)$$

where θ is the angle between the observation direction and the axis normal to the OPA axis, A_n is the optical field amplitude radiated by the n_{th} OPA element, k is the wavenumber, and d and $\Delta\phi$ are the spacing and phase difference between the adjacent OPA elements, respectively. $AF(\theta)$ is a function of the d, frequency f_{ML}, amplitude A_n, and phase ϕ_n of the OPA elements. The side lobes in the far-field beam pattern can be controlled by appropriately assigning the element position, frequency, and field magnitude. Beam steering can be achieved by changing the phase difference between the elements. Therefore, side lobe modulation and beam steering can be achieved at the same time through simultaneous AM/PM. The key mechanism of simultaneous AM/PM to achieve dual function can be realized by modulating the two locking parameters in the OIL lasers, as analyzed by the OIL rate equations [19]:

$$\frac{dA(t)}{dt} = \frac{1}{2}g[N(t) - N_{th}]A(t) + \kappa A_{ML}\cos(\phi(t)), \quad (2)$$

$$\frac{d\phi(t)}{dt} = \frac{\alpha}{2}\{g[N(t) - N_{th}] - \gamma_p\} - \kappa\frac{A_{ML}}{A(t)}\sin(\phi(t)) - 2\pi\Delta f, \quad (3)$$

$$\frac{dN(t)}{dt} = J_{bias}(t) - \gamma_n N(t) - \{\gamma_p + g[N(t) - N_{th}]\}A(t)^2, \quad (4)$$

where $N(t)$ is the carrier number of the SL. g, N_{th}, α, γ_n, and γ_p are the linear gain coefficient, threshold carrier number, linewidth enhancement factor, carrier recombination rate, and photon decay rate of the slave laser, respectively. κ is the field coupling rate between SL and ML. The number of electrons, $J_{bias}(t)$, represents the bias current of the SL in Equation (4). The rate Equations (2)–(4) are solved for the steady-state amplitude $A_{free,SL}$, phase ϕ_n, expressed by [18]:

$$A_{free,SL}^2 = \frac{J_{bias} - \gamma_n N_{th}}{\gamma_p}, \quad (5)$$

$$A_n^2 = \frac{A_{free,SL}^2 - \left(\frac{\gamma_n}{\gamma_p}\right)(N_n - N_{th})}{1 + \left(g[N_n - N_{th}]/\gamma_p\right)}, \quad (6)$$

$$\phi_n = \sin^{-1}\left\{-\frac{2\pi\Delta f}{\kappa\sqrt{(1+\alpha^2)}}\frac{A_n}{A_{ML}}\right\} - \tan^{-1}\alpha. \quad (7)$$

The dependence of the locked-amplitude A_n and phase ϕ_n on the detuning frequency and injection ratio is revealed by Equations (5)–(7). A stable locking regime can be calculated as a function of the injection ratio and detuning frequency. When the OIL laser system operates in the injection-locked region, the SL output is locked to the ML, indicating the frequency and phased locking of the SL to the ML.

We numerically calculated and demonstrated the simultaneous modulation of the amplitude and phase of an OIL output signal in the amplitude-locking and phase-locking maps, which are functions of the detuning frequency and injection ratio, as shown in Figure 3a,b, respectively. The simulation parameters were obtained from [19].

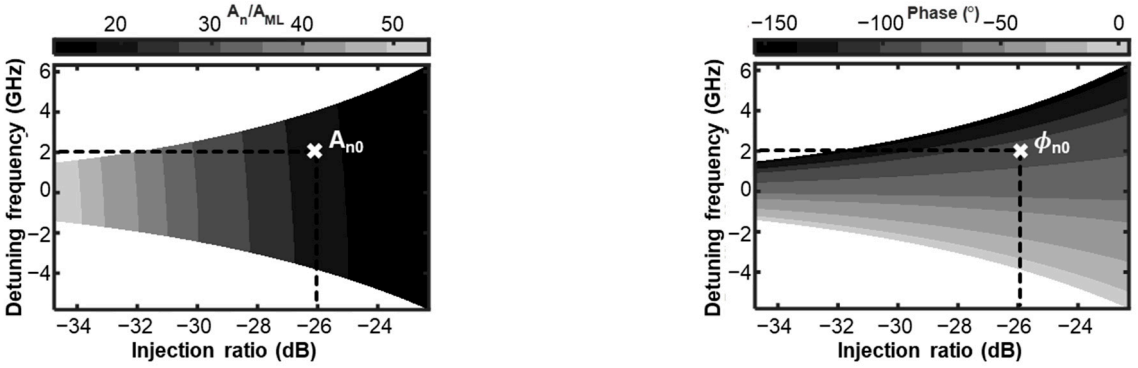

Figure 3. Simultaneous AM/PM on (**a**) amplitude- and (**b**) phase-locking maps as a function of detuning frequency and injection ratio.

The grey-colored regions in Figure 3a,b represent the stable-locked states, in which the frequency of the OIL output signal is locked and equal to ML, while the amplitude and phase are stable. Each pair of OIL parameters within the stable locking region corresponds to a specific pair of amplitude and phase values. For instance, with a detuning frequency of 2 GHz and an injection ratio of −26 dB, we obtained amplitude A_{n0} and phase ϕ_{n0} as shown in Figure 3a,b, respectively. We can extract a specific combination of amplitude and phase by analyzing the locking map shown in Figure 3. Specifically, the appropriate selection of the injection-locking parameters in this locking regime provides a method for controlling the phase and magnitude of the SL. Consequently, by varying the injection-locking parameters, the amplitudes and phases of the OIL lasers can be simultaneously modulated to achieve the required values because of the dependence on both the amplitude and phase. The simultaneous control of the injection-locking parameters can be obtained by directly modulating the bias current of the semiconductor SL owing to the dependence of the output power and frequency on its bias current [20,21]. Therefore, the direct modulation of OIL lasers without external modulators can simplify the OPA system and achieve a low loss, high power efficiency, and noise reduction.

Figure 4a shows the injection-locking parameters for the 21 OIL lasers in the OIL-based OPA. The injection lock positions in the locking map are selected to construct a far-field pattern to modulate the SLLs for broadcasting the OWC, as shown in Figure 4b. First, we calculate the required amplitude and phase profiles of the OPA elements using Equation (1). Subsequently, we look up the corresponding injection parameters on the two locking maps (Figure 3a,b), which relate the required amplitudes and phases of the OIL-based OPA elements. In our simulation, we choose a 5 dB variation to send "1" and "0" bits (e.g., −20 dB for "1" and −25 dB for "0"). The cross and square markers represent the injection-locking parameters of the 21 OIL lasers to achieve SLLs of −20 dB and −25 dB, respectively. By properly controlling the 21 OIL lasers in accordance with the injection-locking parameters, the levels of the entire side lobe were simultaneously modulated while maintaining the same main beam power for the LiDAR function. Figure 4b shows the corresponding far-field beam pattern of the dual-function OPA for a 10 Gbps broadcasting OWC.

Figure 5 shows the results for the directional OWC. The OWC receivers should be located at −40° and 50° directions. The SLLs are modulated between −20 dB and −25 dB to represent "1" and "0" bits of data, respectively. Similar to the broadcasting OWC case, the required injection-locking parameters of the 21 OIL-based OPA elements were calculated and analyzed using locking maps. Figure 5a demonstrates the sets of the cross and square markers that represent the cases of −20 dB and −25 dB of SLLs at −40° and 50° directions, respectively. Figure 5b shows the corresponding far-field beam patterns. The two side lobes in the positions of OWC receivers are modulated between −20 dB and −25 dB, whereas others are maintained at −20 dB. We can achieve SLL modulation at any

specific position of the OWC receiver within the side lobe region for a dual-function OPA. The main beam power is maintained for ranging and sensing operations.

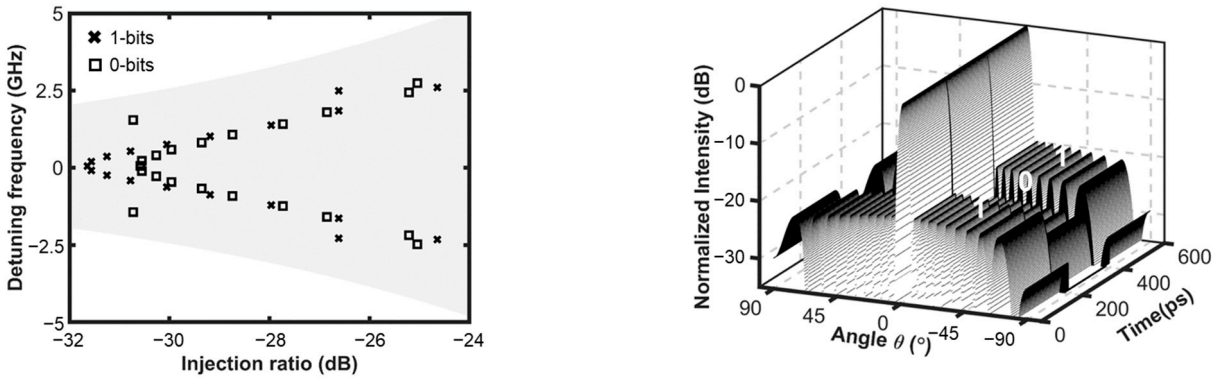

(**a**) (**b**)

Figure 4. (**a**) Control of 21 OIL lasers on locking map and (**b**) corresponding far-field radiation pattern of broadcasting case.

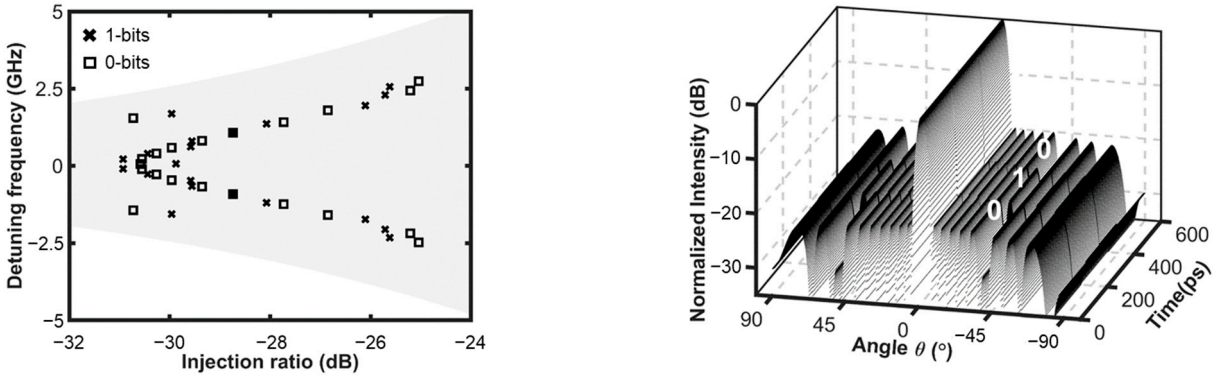

(**a**) (**b**)

Figure 5. (**a**) Controls of 21 OIL lasers on locking map and (**b**) corresponding far-field radiation pattern of directional OWC.

We simulated the eye patterns of the ideal OWC receivers in the steering direction, as shown in Figures 6 and 7. The simulation employed the ordinary differential equation solver in MATLAB on the OIL rate Equations (2)–(4) to obtain the time-domain amplitude and phase of the OIL outputs. The data sequences were generated pseudo-randomly at a rate of 10 Gbps, and the other simulation parameters were obtained from [19].

Figure 6 shows the eye patterns in the broadcast OWC case. Because all the side lobes were modulated, we checked the eye patterns in the $-40°$, $-20°$, $30°$, and $50°$ directions. Although there is a slight difference between the four eye patterns, we can achieve wide-opening eye patterns in any OWC direction because of the high modulation bandwidth of the OIL lasers. The OIL laser exhibited an enhanced modulation performance owing to its increased resonant frequency [17,19]. The high performance of eye patterns ensures reliable data transmission of the broadcasting function using a dual-function OIL-based OPA.

Figure 7a,b shows the eye patterns of 10 Gbps data at $-40°$ and $50°$ in the directional OWC case. We observed the opening of the eye patterns, ensuring the reliability of data transmission, although the phase change of the OPA elements to control the specific side lobes caused a degradation in the eye pattern performance compared with the broadcasting OWC case.

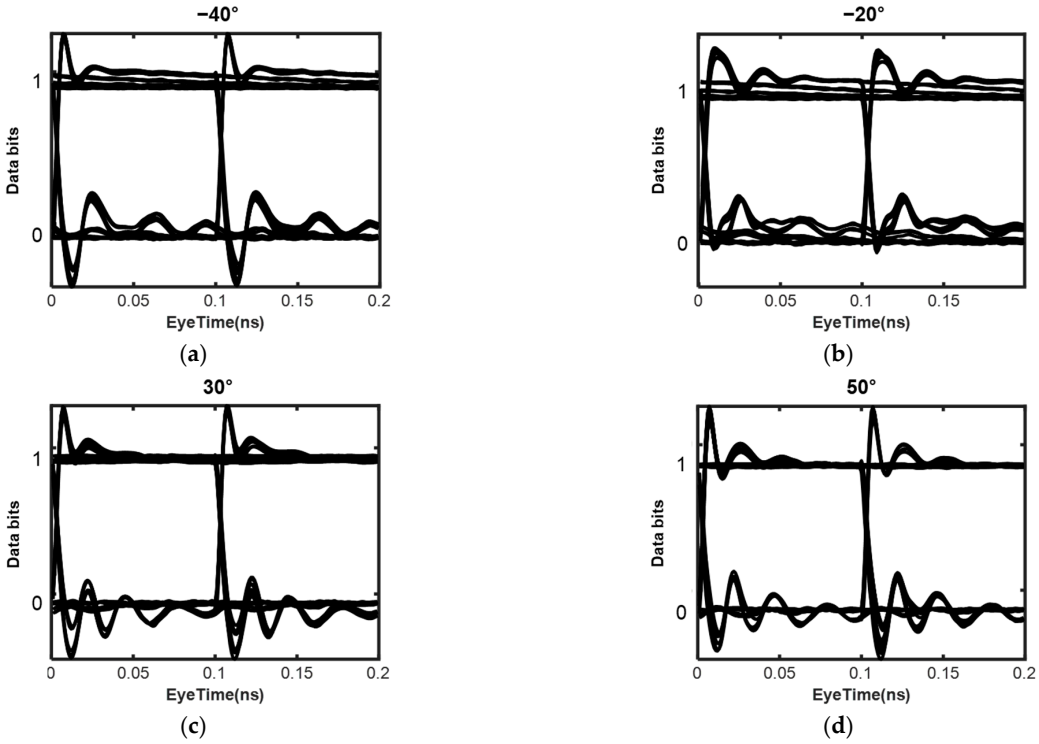

Figure 6. Eye patterns of broadcasting at (**a**) −40°, (**b**) −20°, (**c**) 30°, and (**d**) 50° directions within side lobe regions of the far-field beam pattern.

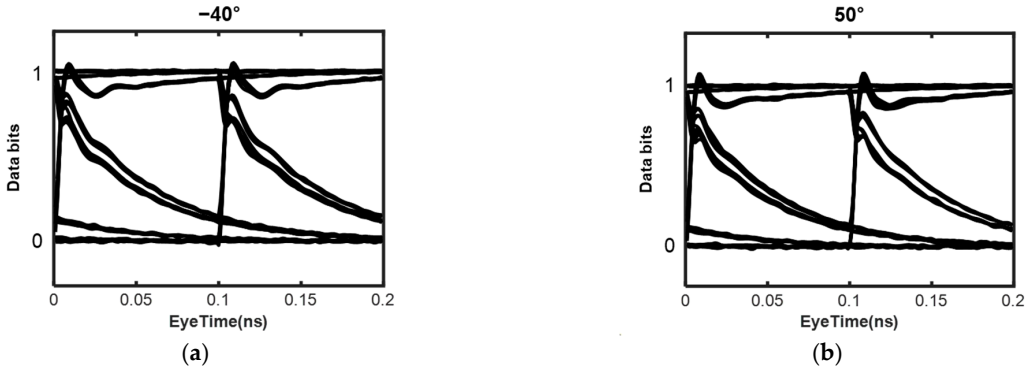

Figure 7. Eye patterns of directional OWC at (**a**) −40° and (**b**) 50° directions of OWC receivers in side lobe regions.

To provide a more comprehensive demonstration, we also investigated the OWC performance at different main beam steering angles for LiDAR applications. In Figure 8, we demonstrate the operation of the dual-function OPA when the LiDAR function steers the beam to 0°. The controls of the 21 OPA elements follow two sets of OIL parameters, which are calculated and presented in Figure 8a. We achieved the corresponding far-field beam patterns in which the side lobes at 50° and −40° directions are magnitude-modulated for OWC applications while maintaining the main beam power for LiDAR, as shown in Figure 8b. The cross markers indicate the set of OIL parameters to obtain the 0 and 1 bits at 50° and −40°, respectively, while the square markers are for the case of 1 and 0 bits assigned at the same directions. Additionally, we simulated and achieved clear eye patterns of 10 Gbps data at the two OWC directions, as demonstrated in Figure 8c,d. Therefore, the dual-function OPA system, using OIL semiconductor lasers, can ensure high OWC performance in side lobes under different LiDAR operation conditions. In addition, the OIL-based OPA offers power scaling capabilities due to the high output power of active emitters, specifically OIL lasers [22], which ensure excellent OWC performance in

side lobes for various application ranges. For example, the proposed 21-element OPA, with an output power of 10 dBm per OIL semiconductor laser, will emit a total output power of 23.5 dBm, with the estimated power in the main beam at 20 dBm. As per the assigned 20 dB SLL, the transmitted power in side lobes for OWC applications is 0 dBm, making it suitable for indoor or short-range OWC applications [23]. High-performance requirements for long-range OWC applications can be achieved by using high-power semiconductor lasers (hundreds of milliwatts) [22], adding optical amplifiers, and utilizing high-sensitivity photodetectors at receivers. Consequently, the dual-function OPA based on OIL semiconductor lasers can achieve high performance of the OWC function in the side lobe region while maintaining the primary LiDAR function in the main lobe.

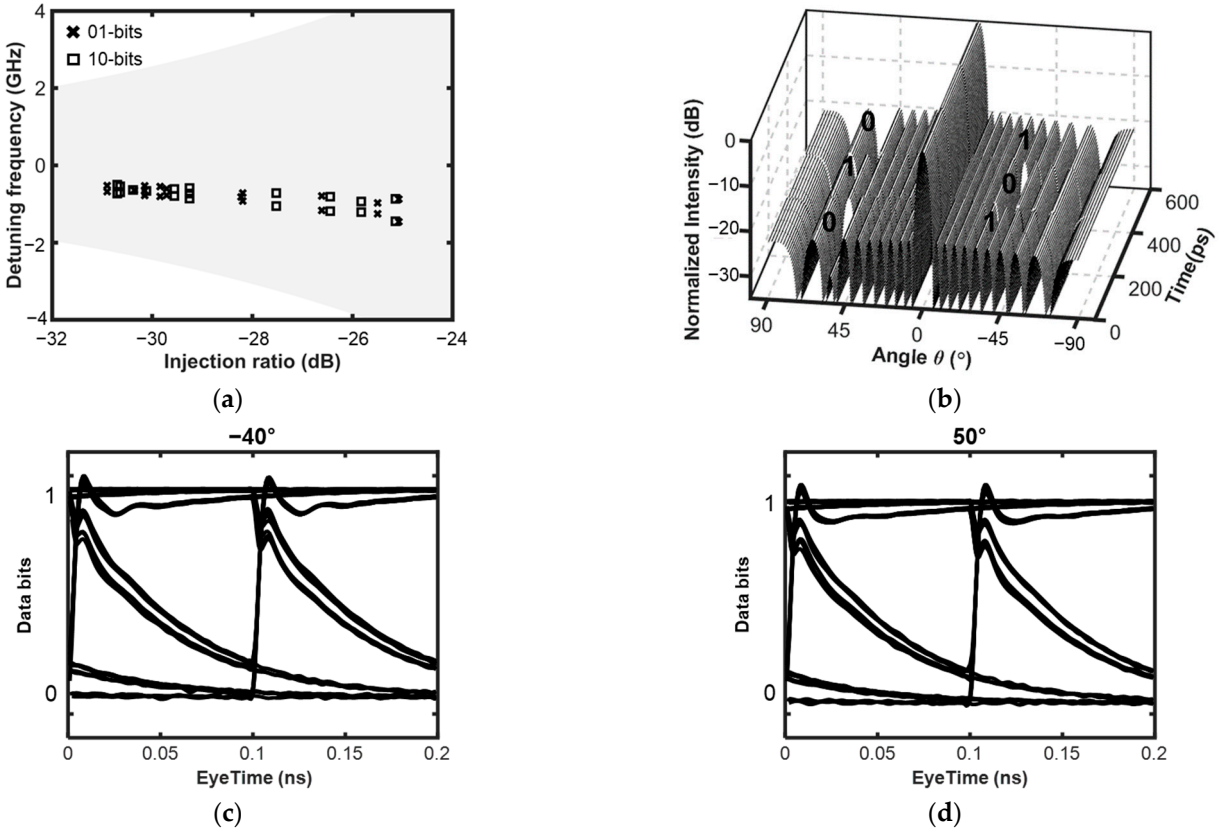

Figure 8. Performance of the OWC function when the LiDAR function steers the beam to 0° direction. (**a**) Controls of 21 OIL lasers on locking map and (**b**) the corresponding far-field radiation pattern with OWC directions at 50° and −40°. Eye patterns at (**c**) −40° and (**d**) 50°.

4. Conclusions

We theoretically proposed and demonstrated a dual-function OPA based on an OIL laser configuration to achieve LiDAR and OWC functions. Simultaneous AM/PM of OIL semiconductor lasers can be achieved through the direct modulation of bias currents on semiconductor SLs. We numerically calculated the amplitudes and phases of the 21 OPA elements required for the modulation of whole side lobes and selected side lobes of OPA beam patterns for the broadcasting and directional OWC cases. We calculated the amplitude and phase values required to achieve the dual functions. We extracted the injection locking parameters for 21 OIL lasers in the OIL-based OPA by analyzing the relationship between the locking map position and signal phase and magnitude. Based on appropriate control of the array phase and amplitude, we generated a far-field beam pattern exhibiting SLL modulations. Clear and reliable eye patterns for 10 Gbps data were demonstrated for both broadcast and directional OWC cases while maintaining the main beam LiDAR operation. In this study, we employed the modulation technique based on the magnitude variation

of side lobes to implement the OWC function. Using the phase modulation technique on side lobe signals may increase the transmission capacity of OWC function, which might be investigated in future research. Dual-function OPA based on OIL semiconductor lasers can be used in various applications, such as autonomous vehicles, drones, and mobile robots employed in civil, military, medical, and agricultural fields, owing to their simplicity and multifunctionality.

Author Contributions: Conceptualization, A.-H.N. and H.-K.S.; simulation, A.-H.N. and H.-S.J.; analysis, A.-H.N., H.-S.J., H.S. and H.-K.S.; writing—original draft preparation, A.-H.N.; writing—review and editing, H.S. and H.-K.S.; visualization, H.S. and H.-K.S.; supervision, H.-K.S. All authors have read and agreed to the published version of the manuscript.

Funding: This work was funded by the National Research Foundation of Korea (NRF) under the Basic Science Research Program (grant number NRF-2021R1F1A1045919).

Institutional Review Board Statement: Not applicable.

Informed Consent Statement: Not applicable.

Data Availability Statement: Not applicable.

Conflicts of Interest: The authors declare no conflict of interest. The funders had no role in the study design, collection, analyses, interpretation of data, writing of the manuscript, or the decision to publish the results.

References

1. Heck, M.J.R. Highly Integrated Optical Phased Arrays: Photonic Integrated Circuits for Optical Beam Shaping and Beam Steering. *Nanophotonics* **2016**, *6*, 93–107. [CrossRef]
2. Guo, Y.; Guo, Y.; Li, C.; Zhang, H.; Zhou, X.; Zhang, L. Integrated Optical Phased Arrays for Beam Forming and Steering. *Appl. Sci.* **2021**, *11*, 4017. [CrossRef]
3. Lin, S.; Chen, Y.; Wong, Z.J. High-Performance Optical Beam Steering with Nanophotonics. *Nanophotonics* **2022**, *11*, 2617–2638. [CrossRef]
4. Chowdhury, M.Z.; Hossan, M.T.; Islam, A.; Jang, Y.M. A Comparative Survey of Optical Wireless Technologies: Architectures and Applications. *IEEE Access* **2018**, *6*, 9819–9840. [CrossRef]
5. Sun, J.; Timurdogan, E.; Yaacobi, A.; Hosseini, E.S.; Watts, M.R. Large-Scale Nanophotonic Phased Array. *Nature* **2013**, *493*, 195–199. [CrossRef] [PubMed]
6. Sayyah, K.; Efimov, O.; Patterson, P.; Schaffner, J.; White, C.; Seurin, J.-F.; Xu, G.; Miglo, A. Two-Dimensional Pseudo-Random Optical Phased Array Based on Tandem Optical Injection Locking of Vertical Cavity Surface Emitting Lasers. *Opt. Express* **2015**, *23*, 19405. [CrossRef] [PubMed]
7. Poulton, C.V.; Yaacobi, A.; Cole, D.B.; Byrd, M.J.; Raval, M.; Vermeulen, D.; Watts, M.R. Coherent Solid-State LIDAR with Silicon Photonic Optical Phased Arrays. *Opt. Lett.* **2017**, *42*, 4091. [CrossRef]
8. Lesina, A.C.; Lesina, A.C.; Lesina, A.C.; Lesina, A.C.; Lesina, A.C.; Lesina, A.C.; Goodwill, D.; Bernier, E.; Ramunno, L.; Ramunno, L.; et al. On the Performance of Optical Phased Array Technology for Beam Steering: Effect of Pixel Limitations. *Opt. Express* **2020**, *28*, 31637–31657. [CrossRef]
9. Zhang, X.; Kwon, K.; Henriksson, J.; Luo, J.; Wu, M.C. A Large-Scale Microelectromechanical-Systems-Based Silicon Photonics LiDAR. *Nature* **2022**, *603*, 253–258. [CrossRef]
10. Poulton, C.V.; Byrd, M.J.; Russo, P.; Timurdogan, E.; Khandaker, M.; Vermeulen, D.; Watts, M.R. Long-Range LiDAR and Free-Space Data Communication with High-Performance Optical Phased Arrays. *IEEE J. Sel. Top. Quantum Electron.* **2019**, *25*, 1–8. [CrossRef]
11. Sacher, W.D.; Chen, F.-D.; Moradi-Chameh, H.; Liu, X.; Felts Almog, I.; Lordello, T.; Chang, M.; Naderian, A.; Fowler, T.M.; Segev, E.; et al. Optical Phased Array Neural Probes for Beam-Steering in Brain Tissue. *Opt. Lett.* **2022**, *47*, 1073. [CrossRef] [PubMed]
12. Scotti, F.; Onori, D.; Porzi, C.; Falconi, F.; Sorianello, V.; Alves, A.; Imran, M.; Pinna, S.; Cerqueira, A.; Romagnoli, M.; et al. Dual Use Architecture for Innovative Lidar and Free Space Optical Communications. *Appl. Opt.* **2017**, *56*, 8811. [CrossRef]
13. Wild, T.; Braun, V.; Viswanathan, H. Joint Design of Communication and Sensing for beyond 5G and 6G Systems. *IEEE Access* **2021**, *9*, 30845–30857. [CrossRef]
14. Kang, M.; Baek, J. Efficient and Accurate Synthesis for Array Pattern Shaping. *Sensors* **2022**, *22*, 5537. [CrossRef] [PubMed]
15. Nguyen, A.H.; Cho, J.-H.; Bae, H.-J.; Sung, H.-K. Side-Lobe Level Reduction of an Optical Phased Array Using Amplitude and Phase Modulation of Array Elements Based on Optically Injection-Locked Semiconductor Lasers. *Photonics* **2020**, *7*, 20. [CrossRef]
16. Nguyen, A.-H.; Cho, J.-H.; Sung, H.-K. Theoretical Demonstration of Security Improvement of Optical Phased Array Based on Optically Injection-Locked Lasers. *Photonics* **2021**, *8*, 469. [CrossRef]

17. Lau, E.K.; Wong, L.J.; Wu, M.C. Enhanced modulation characteristics of optical injection-locked lasers: A tutorial. *IEEE J. Sel. Top. Quantum Electron.* **2009**, *15*, 618–633. [CrossRef]
18. Balanis, C.A. Arrays: Linear, Planar, and Circular. In *Antenna Theory Analysis and Design*, 3rd ed.; John Wiley and Sons: Hoboken, NJ, USA, 2005; pp. 283–384.
19. Lau, E.K.; Sung, H.-K.; Wu, M.C. Frequency Response Enhancement of Optical Injection-Locked Lasers. *IEEE J. Quantum Electron.* **2008**, *44*, 90–99. [CrossRef]
20. Lee, H.; Cho, J.-H.; Sung, H.-K. Theoretical Analysis of a Method for Extracting the Phase of a Phase-Amplitude Modulated Signal Generated by a Direct-Modulated Optical Injection-Locked Semiconductor Laser. *Opt. Eng.* **2017**, *56*, 056112. [CrossRef]
21. Cho, J.-H.; Cho, C.-H.; Sung, H.-K. Theoretical Performance Evaluation of Optical Complex Signals Based on Optically Injection-Locked Semiconductor Lasers. *IEEE J. Sel. Top. Quantum Electron.* **2019**, *25*, 1–9. [CrossRef]
22. Shimasaki, T.; Edwards, E.R.; DeMille, D. Injection-Locking of a Fiber-Pigtailed High-Power Laser to an External Cavity Diode Laser via a Fiber Optic Circulator. *Rev. Sci. Instrum.* **2019**, *90*, 056102. [CrossRef] [PubMed]
23. Rhee, H.-W.; You, J.-B.; Yoon, H.; Han, K.; Kim, M.; Lee, B.G.; Kim, S.-C.; Park, H.-H. 32 Gbps Data Transmission with 2D Beam-Steering Using a Silicon Optical Phased Array. *IEEE Photonics Technol. Lett.* **2020**, *32*, 803–806. [CrossRef]